

# THREE-DIMENSIONAL MAPPING OF CDM SUBSTRUCTURE AT SUBMILLIMETER WAVELENGTHS

KAIKI TARO INOUE<sup>1</sup> AND MASASHI CHIBA<sup>2</sup>

*Draft version September 19, 2018*

## ABSTRACT

The cold dark matter (CDM) structure formation model predicts that about 5-10 % of a typical galactic halo of mass  $\sim 10^{12}M_{\odot}$  is in substructures with masses  $\lesssim 10^8M_{\odot}$ . To directly detect such substructures, we propose to observe dust continuum emission from a strongly lensed QSO-host galaxy using a large submillimeter interferometer array with a high angular resolution of  $\sim 0.01$ arcsec such as the planned Atacama Large Submillimeter Array (ALMA). To assess their observational feasibility, we numerically simulate millilensing of an extended circular source by a CDM substructure modeled as a tidally truncated singular isothermal sphere (SIS) embedded in a typical QSO-galaxy lens system, B1422+231, modeled as a singular isothermal ellipsoid (SIE) with an external constant shear and a constant convergence. Assuming an angular resolution of 0.01arcsec, we find that the angular positions of  $\sim 10^8M_{\odot}$  substructures at several kpc from the center of the macrolens halo can be directly measured if the size of the dust continuum emission region and the gradient of the surface brightness at the position of the perturber are sufficiently large. From the astrometric shift on a scale of a few times 10 mas of an image perturbed by a subhalo with respect to an unperturbed macrolensed image, we can break the degeneracy between subhalo mass and distance provided that macrolensing parameters are determined from positions and fluxes of multiple images.

*Subject headings:* cosmology: theory – dark matter – gravitational lensing – large-scale structure of universe

## 1. INTRODUCTION

Recent high-resolution  $N$ -body simulations of the cold dark matter (CDM) structure formation model show an excess in the number of subhalos (“substructures”) in a galaxy-sized halo in comparison with the number of Milky Way or M31 satellites (Klypin et al. 1999; Moore et al. 1999). If the CDM-based structure formation scenario is the correct one, then we expect a large number of invisible satellites inside a halo of galaxies.

Currently, gravitational lensing is the only probe that can test the abundance of these invisible satellites or equivalently, substructures in a galaxy-sized halo. In fact, gravitationally multiply lensed QSOs have recently been used for putting limits on the surface density and the mass of such invisible substructures (Mao & Schneider 1998; Metcalf & Madau 2001; Chiba 2002; Metcalf & Zhao 2002; Dalal & Kochanek 2002; Bradac et al. 2002). Statistical analyses on these quadruple QSO-galaxy lensing systems that show an anomalous flux ratio imply the presence of substructures along the line-of-sight to the multiple images (Metcalf & Zhao 2002; Evans & Witt 2003; Keeton, et al. 2003).

However, the location of a subhalo along the line-of-sight is poorly constrained. In fact, more massive extragalactic  $10^8 - 10^9M_{\odot}$  halos along the line-of-sight to the multiple images may also significantly contribute to altering the flux ratio of multiple images (Metcalf 2005). In order to determine the distances to these subhalos, we need to have more information in addition to the position and flux of multiple images (Yonehara, et al. 2003).

To directly map out the three-dimensional locations

of  $10^8M_{\odot}$  invisible subhalos, we propose to observe the dust continuum emission from a strongly lensed QSO-host galaxy using a large submillimeter interferometer array with a high angular resolution of  $\sim 0.01$  arcsec such as the ALMA.

Recent submillimeter observations revealed that about 60 % of strongly lensed active galactic nuclei (AGNs) are luminous at a submillimeter wavelength of  $850\mu\text{m}$  (Barvainis & Ivison 2002) implying that a large amount of energy emitted by stars and AGNs in the QSO host galaxy has been absorbed by dust grains and then re-radiated at longer wavelengths. The dust is heated to temperatures of 20-50K and radiates as a modified blackbody at far-infrared wavelengths (Wiklind 2003). At a redshift  $z \simeq 3 - 4$ , the corresponding energy peak is at a submillimeter wavelength  $\sim 0.1$  mm. The region responsible for this dust continuum emission has a typical scale of  $10^2$ pc to a few kpc. Therefore, the effects of an extended source with an angular size larger than the Einstein radius of a perturber will be easily observed at submillimeter wavelengths (Blain 1999; Wiklind & Alloin 2002).

In this paper, we show our simulation results of millilensing of an extended circular source by a CDM substructure whose Einstein radius is smaller than the source size. We also show that the astrometric shifts of images perturbed by a subhalo can reveal the three-dimensional position of a subhalo along the line-of-sight. As an example, we choose a typical QSO-galaxy lensing system, B1422+231, with cusp-caustics in order to check the observational feasibility of mapping substructures.

## 2. SIMULATION

The typical QSO-galaxy lensing system B1422+231 shows an anomalous flux ratio. The images consist of three highly magnified images A, B, and C, and a faint one D located near the lens galaxy. The observed

arXiv:astro-ph/0503212v3 5 Oct 2005

<sup>1</sup> Department of Science and Engineering, Kinki University, Higashi-Osaka, 577-8502, Japan

<sup>2</sup> Astronomical Institute, Tohoku University, Sendai 980-8578, Japan

mid-infrared flux ratios are  $A/|B| = 0.94 \pm 0.05$  and  $C/|B| = 0.57 \pm 0.06$  (Chiba et al. 2005). The radio and optical flux ratios are consistent with the mid-infrared values within a  $\sim 10\%$  error. If we assume that the gravitational potential of the macrolens is a smooth one, we expect a cusp-caustic relation in the flux ratio,  $f \equiv (A + B + C)/(|A| + |B| + |C|) = 0$ . However, B1422+231 shows a 20% deviation from the  $f = 0$  relation. Assuming that such an anomaly is caused by the presence of an SIS perturber in the macrolens halo, the anomaly might be in image A (Dobler & Keeton 2005). The redshifts of the source and the lens are  $z_S = 3.62$  and  $z_L = 0.34$ , respectively. In what follows, we assume the following cosmological parameters: the present density of matter  $\Omega_m = 0.3$ , the present density of the cosmological constant  $\Omega_\Lambda = 0.7$ , and the Hubble parameter  $h = 0.7$ , which yield the angular diameter distances to the lens and to the source,  $D_L = 1.00$  Gpc and  $D_S = 1.49$  Gpc, respectively.

To model the macrolens system, we adopt an SIE in an external shear field in which the isopotential curves in the projected surface perpendicular to the line-of-sight are ellipses (Kormann et al. 1994). For further details, see Chiba (2002). In what follows, we assume an angular resolution of 0.01 arcsec which will be achieved by the planned ALMA at 850  $\mu\text{m}$ . Because the Einstein radius for an SIS with a one-dimensional velocity dispersion  $\sigma$  at  $D_L = 1.00$  Gpc and  $D_S = 1.49$  Gpc is

$$\theta_{Ep} = 1.0 \times 10 \left( \frac{\sigma}{21 \text{ km s}^{-1}} \right)^2 \text{ mas}, \quad (1)$$

observation with an angular resolution of 0.01 arcsec will reveal subhalos with a one-dimensional velocity dispersion  $\sigma \gtrsim 20 \text{ km s}^{-1}$  for B1422+231.

As a model of a CDM subhalo, we consider a spherically symmetric, tidally truncated SIS with one-dimensional velocity dispersion  $\sigma$ . At a distance  $r$  from the center of a macrolens galactic halo with a one-dimensional velocity dispersion  $\sigma_0$ , the tidal radius is approximately given by  $r_t \approx r\sigma/\sigma_0$ . For an SIS with a one-dimensional velocity dispersion  $\sigma \sim 20 \text{ km s}^{-1}$ , the tidally truncated mass is  $M_{\text{SIS}} \sim 10^8 M_\odot$ . Provided that the mass function for subhalos satisfies  $dn/dM \propto M^{-2}$ , as many  $N$ -body simulations suggest (e.g., Klypin et al. 1999), the differential lensing cross section  $dS$  per logarithmic mass interval is  $dS = \theta_{Ep}^2 dn/d \ln M \propto M^{1/3}$  because the area inside an Einstein radius for a tidally cut SIS is  $\theta_{Ep}^2 \propto M_{\text{SIS}}^{4/3}$ . Thus, the contribution of massive subhalos to the substructure lensing is somewhat significant in comparison with that of less massive ones. We also assume that a perturbing subhalo is located at a distance equal to the size of the Einstein radius of the macrolens halo  $r_E = D_L \theta_E = 3.8 \text{ kpc}$  from the macrolens center (where  $\theta_E$  is the Einstein angular radius of the macrolens halo). This assumption can be verified as follows. Consider a column with a unit section centered at a point  $P$  aligned to the line-of-sight direction centered at a distance equal to the size of the Einstein radius of the macrolens  $r_E$  from the macrolens center. We introduce a column distance  $L$  from  $P$  as a coordinate in the direction of the line-of-sight in the column. If the subhalo distance is larger than the size of the Einstein radius of the macrolens halo,  $r \gg r_E$ , the tidally

truncated mass approximately satisfies  $M_{\text{SIS}} \propto L$ , since  $r \sim L$ . Therefore, the probability of having a subhalo with a fixed one-dimensional velocity dispersion  $\sigma$  per logarithmic column distance  $\ln L$  is  $dp(L) \sim L^{-1} d \ln L$ , provided that the mass function for subhalos in the column with a fixed one-dimensional velocity dispersion satisfies  $dn/dM \propto M^{-2}$ . Thus, the lensing probability is expected to be larger for a smaller column distance  $L$ .

If the ‘‘real’’ mass function takes a different form, or the above assumption is incorrect, the perturbing subhalo may reside at a position with a larger column distance  $L > r_E$ . Then the corresponding subhalo mass will be increased by a factor of  $\sim L/r_E$ .

In our simulation, we put a tidally truncated SIS with a mass of  $2 \times 10^8 M_\odot$  near the A image.<sup>3</sup> The corresponding Einstein radius of the SIS is  $\theta_{Ep} \sim 17$  mas. As a model of emission from cold dusts, we assume a circularly symmetric Gaussian source with a standard deviation  $L = 2.5 \times 10^2 \text{ pc}$ .

### 3. RESULT

The left panels in Figure 1 show lensed images without any perturbers, whereas the right panels show those perturbed by an SIS perturber. As shown in a zoomed in picture of image A (*top right*), the angular position of an SIS can be clearly identified by a dipole structure that consists of a pair of dark and bright spots at the place where the surface brightness gradient is non-vanishing (Inoue & Chiba 2003). One can also notice that shifts of an image outside the Einstein radius  $\theta_{Ep}$  of an SIS with respect to the unperturbed macrolensed image are significantly suppressed (*top right*).

If we can approximate the lens system near the perturber locally as an SIS plus a constant shear  $\gamma$  and a constant convergence  $\kappa$ , then the lens equation normalized by the Einstein radius  $\theta_{Ep}$  of an SIS in the coordinates aligned to the shear can be written in terms of a source position  $\mathbf{y} = (y_1, y_2)$  and an image position  $\mathbf{x} = (x_1, x_2)$  as

$$\mathbf{y} = (\mathbf{1} - \mathbf{\Gamma})\mathbf{x} - \frac{\mathbf{x}}{|\mathbf{x}|}, \quad (2)$$

where

$$\mathbf{\Gamma} = \begin{pmatrix} \kappa + \gamma & 0 \\ 0 & \kappa - \gamma \end{pmatrix}. \quad (3)$$

Let  $\mathbf{x}_0 = (x_{01}, x_{02})$  be the image position for a macrolens model without any perturbers. In terms of the polar coordinates  $(R_p, \phi)$  defined as  $\mathbf{x} = (R_p \cos \phi, R_p \sin \phi)$ , the lens equation (2) yields

$$x_{01}^2 (R_p - \xi_2^{-1})^2 + x_{02}^2 (R_p - \xi_1^{-1})^2 = (R_p - \xi_1^{-1})^2 (R_p - \xi_2^{-1})^2, \quad (4)$$

where  $\xi_1 \equiv 1 - \kappa - \gamma$  and  $\xi_2 \equiv 1 - \kappa + \gamma$ . The astrometric shift  $\Delta \mathbf{x} \equiv \mathbf{x} - \mathbf{x}_0$  as a function of  $\mathbf{x}_0$  can be obtained by solving the fourth-order equation (4) with equation (2) analytically. For a positive parity case  $\xi_1 > 0, \xi_2 > 0$ , an image at a horizontal axis  $(x_{01}, 0)$  is shifted to  $(x_{01} + \xi_1^{-1}, 0)$ , whereas an image at a vertical axis

<sup>3</sup> We choose an appropriate position of the SIS that approximately gives the observed anomaly flux ratio, but we did not fix the relative position of the images in a small source size limit. Therefore, our simulation should be interpreted as a demonstration of extended source size effects rather than that of a best-fit model.

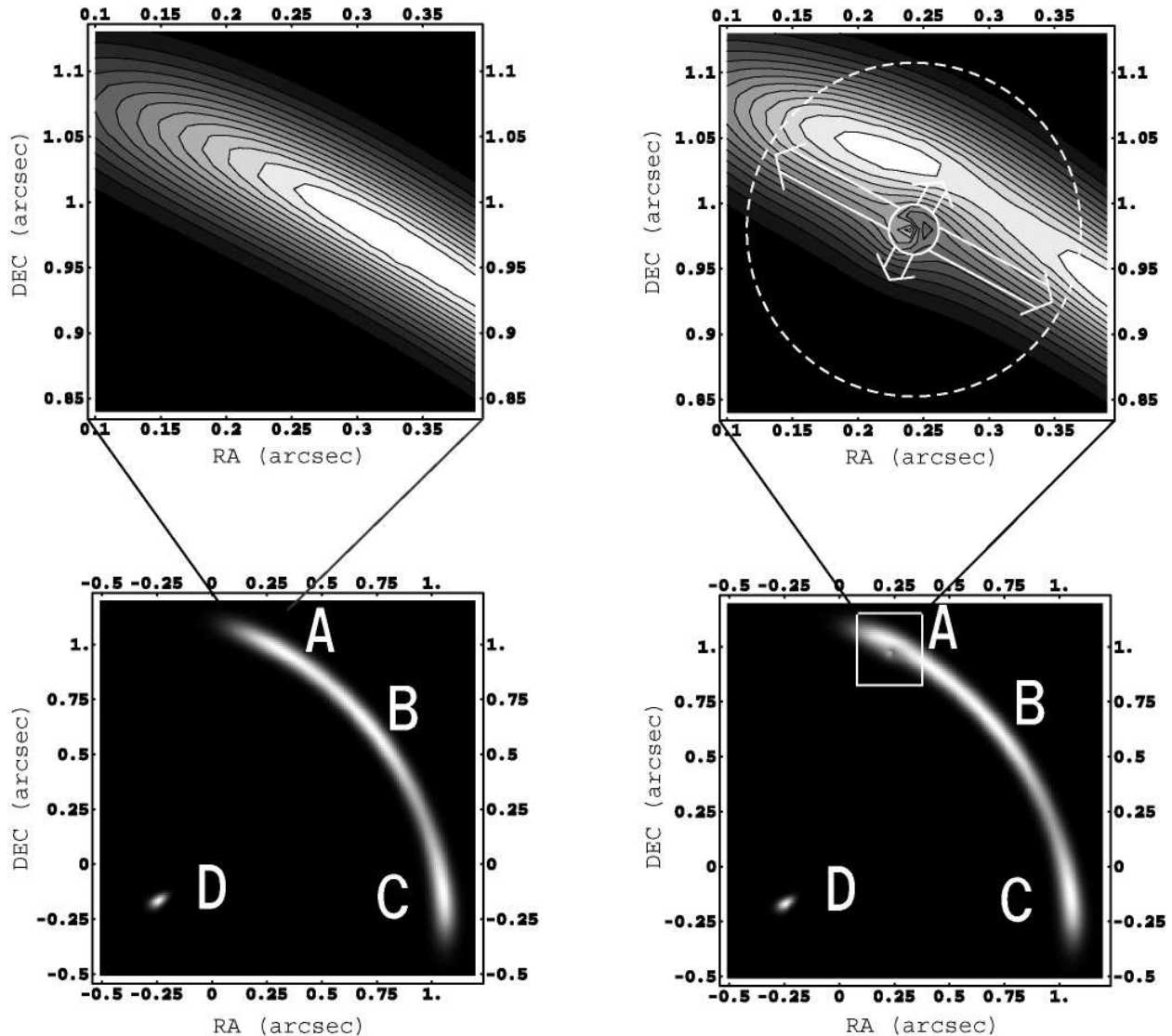


FIG. 1.— Simulated images of B1422+231 at submillimeter wavelengths without any perturbers (*left*) and with an SIS perturber (*right*) for a Gaussian circular source with a standard deviation  $L = 2.5 \times 10^2$  pc. A tidally truncated SIS with a mass of  $2 \times 10^8 M_\odot$  is put at the center of a thick circle (*top right*) near the A image. The dashed circle represents a circle with the tidal radius centered at an SIS perturber. The angular resolution is assumed to be 0.01 arcsec. Astrometric shifts in the tangential direction and those in the radial direction in the coordinates aligned to the shear are represented by arrows.

$(0, x_{02})$  is shifted to  $(0, x_{02} + \xi_2^{-1})$  (Inoue & Chiba 2004). One can see in the top right panel in figure 1 that image A, with positive parity  $\kappa \sim 0.38, \gamma \sim 0.47$ , is largely stretched in the tangential direction by  $\xi_1^{-1} \sim 6.7$  and slightly stretched in the radial direction by  $\xi_2^{-1} \sim 0.92$  with respect to the center of the perturber. The astrometric shift is significantly suppressed if the lensed image is placed outside the tidal radius centered at the SIS perturber, because the projected gravitational potential decreases faster, as  $R^{-1}$ , than an SIS without truncation, where  $R$  is the projected distance from the center of the SIS. If the redshift and the one-dimensional velocity dispersion  $\sigma_0$  of the macrolens halo are known, then we obtain the tidal radius as a function of the distance from the center of the macrolens halo. From the observed angular size for which the astrometric shifts are significantly suppressed, we can determine the distance from the center of the lens halo, in principle.

Next, we show that a measurement of astrometric shifts can break the degeneracy between substructure mass and distance in the line-of-sight to the image. Consider a halo at redshift  $z = z_h$  and a clump (a substructure) in the foreground of the halo at redshift  $z_c < z_h$ . Let  $D_s, D_{ch}, D_{cs}$ , and  $D_h$  be the angular diameter distances to the source, between the clump and halo, between the clump and source, and to the halo, respectively. Provided that the angle between the perturber and the macrolensed image is sufficiently small in comparison with the Einstein radius of the macrolens  $\theta_E$ , the effective lens equation for an SIS plus a constant shear and a constant convergence can be written as (Keeton 2003)

$$\tilde{\mathbf{y}} = (1 - \tilde{\Gamma})\mathbf{x} - \frac{\mathbf{x}}{|\mathbf{x}|}, \quad (5)$$

where  $\tilde{\mathbf{y}} = (1 - \beta\Gamma)^{-1}\mathbf{y}$ ,  $\tilde{\Gamma} = \mathbf{1} - (1 - \beta\Gamma)^{-1}(\mathbf{1} - \Gamma)$ , and

$\beta = D_{ch}D_s/D_{cs}D_h$ . Because an effective unperturbed image position  $\tilde{\mathbf{x}}_0$  that satisfies  $\tilde{\mathbf{y}} = (\mathbf{1} - \tilde{\mathbf{\Gamma}})\tilde{\mathbf{x}}_0$  is equal to the unperturbed macrolensed image position  $\mathbf{x}_0$ , astrometric shifts can be written as  $\Delta\mathbf{x} = \mathbf{x} - \tilde{\mathbf{x}}_0$ . The effective convergence and shear in  $\tilde{\mathbf{\Gamma}}$  are then (Keeton 2003)

$$\kappa_{\text{eff}} = \frac{(1 - \beta)(\kappa - \beta(\kappa^2 - \gamma^2))}{(1 - \beta\kappa)^2 - \beta^2\gamma^2}, \gamma_{\text{eff}} = \frac{(1 - \beta)\gamma}{(1 - \beta\kappa)^2 - \beta^2\gamma^2}. \quad (6)$$

Thus, astrometric shifts are described in the same manner as in the case when  $\beta = 0$ . A tangential shift is  $\Delta x_1 = (1 - \kappa_{\text{eff}} - \gamma_{\text{eff}})^{-1}$ , and a radial shift is  $\Delta x_2 = (1 - \kappa_{\text{eff}} + \gamma_{\text{eff}})^{-1}$  (Inoue & Chiba 2004). As shown in figure 2, for images with positive parity, the tangential shift decreases as the distance between a perturber and a macrolens halo increases. As the distance to the clump  $D_c$  decreases, the astrometric shift becomes less conspicuous and more isotropic. In fact, in the limit  $D_c \rightarrow 0$  or, equivalently,  $\beta \rightarrow 1$ , the astrometric shifts converge to a perfect isotropic shift  $\Delta\mathbf{x} = \mathbf{x}_0/|\mathbf{x}_0|$ . Thus, the distance between a halo and a clump can be measured by the absolute value and the anisotropy of the shifts, provided that the distances to the macrolens halo  $D_h$  and the source  $D_s$  are known already.

Similarly, we can calculate astrometric shifts  $\Delta\mathbf{x}$  in the background case  $z_c > z_h$ . Again, the effective lens equation takes the same form as in equation (5) (Keeton 2003),

$$\mathbf{y} = (\mathbf{1} - \tilde{\mathbf{\Gamma}})\tilde{\mathbf{x}} - \frac{\tilde{\mathbf{x}}}{|\tilde{\mathbf{x}}|}, \quad (7)$$

where  $\tilde{\mathbf{x}} = (\mathbf{1} - \beta\mathbf{\Gamma})\mathbf{x}$ ,  $\tilde{\mathbf{\Gamma}} = \mathbf{1} - (\mathbf{1} - \mathbf{\Gamma})(\mathbf{1} - \beta\mathbf{\Gamma})^{-1}$ , and  $\beta = D_{ch}D_s/D_cD_{sh}$  ( $D_{sh}$  is the angular diameter distance between the source and the halo). We can define an effective position of the unperturbed image  $\tilde{\mathbf{x}}_0$  satisfying  $\mathbf{y} = (\mathbf{1} - \tilde{\mathbf{\Gamma}})\tilde{\mathbf{x}}_0$ , which leads to  $\tilde{\mathbf{x}}_0 = (\mathbf{1} - \beta\mathbf{\Gamma})\mathbf{x}_0$ . Then astrometric shifts can be expressed as  $\Delta\mathbf{x} = (\mathbf{1} - \beta\mathbf{\Gamma})^{-1}\Delta\tilde{\mathbf{x}}((\mathbf{1} - \beta\mathbf{\Gamma})\mathbf{x}_0)$ , where  $\Delta\tilde{\mathbf{x}} \equiv \tilde{\mathbf{x}} - \tilde{\mathbf{x}}_0$ . Thus, astrometric shifts in the background case are different from those in the foreground case with the same  $\beta$ , although the effective lens equation takes the same form in both cases. From the right panels in Figure 2 and 3, one can see that the shifts of images near the horizontal axis ( $x_1, 0$ ) are larger for the background case in comparison with the foreground case with the same  $\beta$ . As shown in the left panel in Figure 2 and both panels in Figure 3, the astrometric shifts of images on the horizontal axis  $\Delta\mathbf{x} = (\xi_1^{-1}, 0)$  and those on the vertical axis  $\Delta\mathbf{x} = (0, \xi_2^{-1})$  do not depend on  $\beta$  in the background case. However, astrometric shifts of all the other images do depend on  $\beta$ . As  $\beta$  increases from 0, astrometric shifts tend to become isotropic except for images on the axes of coordinates aligned to the shear, but they cannot be perfectly isotropic as in the foreground case even if  $\beta = 1$ .

Now let us assess our assumption for constancy in the convergence  $\kappa$  and shear  $\gamma$ . The absolute errors in astrometric shifts in the horizontal direction (aligned to the shear) and in the vertical direction are written in terms of absolute errors in the convergence  $\delta\kappa$  and shear  $\delta\gamma$  as  $\delta(\Delta x_1) \sim \xi_1^{-1}(|\delta\kappa/\kappa| + |\delta\gamma/\gamma|)$  and  $\delta(\Delta x_2) \sim \xi_2^{-1}(|\delta\kappa/\kappa| + |\delta\gamma/\gamma|)$ , respectively. In order to achieve a three-dimensional mapping with an angular resolution

of a unit Einstein radius ( $\sim \theta_{E_p} = 1$ ), the errors  $\delta\kappa$  and  $\delta\gamma$  should satisfy  $|\xi_i^{-1}(|\delta\kappa/\kappa| + |\delta\gamma/\gamma|) \ll 1$  ( $i = 1, 2$ ) at the scale of a unit Einstein radius. In order to check this condition, we compute  $\kappa$  and  $\gamma$  in the neighborhood of an SIS perturber for our SIE model. As shown in Figure 4, the variances in  $\kappa$  and  $\gamma$  at the scale of the perturber's Einstein radius  $\theta_{E_p} = 17$  mas are only of the order of a few %. Thus, our approximation is verified for an SIS with one-dimensional dispersion  $\sigma \sim 20$  km s $^{-1}$ . In more general settings, the magnitude of spatial variation in the convergence and shear at the scale of the Einstein radius  $\theta_{E_p}$  of a perturber can be estimated as  $\delta\kappa/\kappa \sim \delta\gamma/\gamma \sim \theta_{E_p}/\theta_E$ . If the macrolens is also an SIS with a one-dimensional velocity dispersion  $\sigma_0$ , then we should have  $\xi_i(\sigma/\sigma_0)^2 \ll 1$ . In our model, this condition is roughly satisfied, because  $\sigma_0 \sim 180$  km s $^{-1}$ . However, for subhalos with a much larger velocity dispersion  $\sigma$ , we should take the effect of spatial variance in the convergence  $\kappa$  and shear  $\gamma$  into account.

#### 4. OBSERVATIONAL FEASIBILITY

The observed values of the flux density at 850 $\mu\text{m}$  of QSOs at  $z = 3 - 4$  with a starburst are typically several tens of mJy, which implies an emission from dust with a temperature of 30-60K from a fairly extended region of  $10^2 - 10^3$  pc (Barvainis & Ivison 2002). Let us assume that the far-infrared dust emission can be represented by a single-temperature graybody emission with a rest-frame spectral energy distribution (SED) (Wiklind 2003)

$$S(\nu_r, T_d) = \Omega B(\nu_r, T_d)(1 - \exp(-(\nu_r/\nu_0)^\beta)), \quad (8)$$

where  $B(\nu_r, T_d)$  is the Planck function in terms of a rest-frame frequency  $\nu_r$  and a dust temperature  $T_d$ ,  $\beta = 1 - 2$  is the model parameter that controls the grain emissivity,  $\nu_0$  is the critical frequency that controls the opacity of the dust, and  $\Omega$  is the solid angle of the source seen by an observer. A rest-frame SED  $S$  is related to the observer-frame SED as  $\tilde{S}(\nu) = S((1+z)\nu, T_d)/(1+z)$ . Assuming a model with  $\beta = 1.5$ ,  $\nu_0 = 6$  THz, a dust temperature  $T_d = 40$  K, and a dust emission region from a circular disk with a radius  $L = 250$  pc, at 850  $\mu\text{m}$ , the observed energy density would be  $\sim 2.6$  mJy.

Because the ratio of the area  $D$  within the Einstein radius of a  $2 \times 10^8 M_\odot$  SIS perturber to the area of image A is approximately 1/50, the observed energy flux from the area  $D$  will be  $\sim 4 \times 10^{-4}$  Jy, taking a magnification factor of  $\sim 6$  into account. In order to measure the difference in the energy flux at the scale of the Einstein radius of the SIS perturber, for a source with a smooth surface brightness distribution (e.g., Gaussian) one needs a sensitivity of at least  $\sim 4 \times 10^{-5}$  Jy. On the other hand, the sensitivity of ALMA at 850  $\mu\text{m}$  for a point source (signal-to-noise ratio S/N= 1) is  $1.2 \times 10^{-5} \times (\text{integration time}/5\text{hour})^{-1/2}$  Jy.<sup>4</sup> Thus, ALMA has a sufficient sensitivity for a source with a spatially varying surface brightness to detect the dipole structure caused by a  $2 \times 10^8 M_\odot$  SIS perturber. The required integration time would be several hours. Intrinsic surface brightness variations in the source might make the identification of the clear dipole structure rather difficult. However, such a difficulty can be avoided by

<sup>4</sup> See the ALMA home page at <http://www.eso.org/projects/alma/science/bin/sensitivity.html>.

comparing multiple macrolensed images, because intrinsic variations in one macrolensed image can be linearly mapped to those in another one.

#### 5. SUMMARY AND DISCUSSION

In this paper, we have proposed a new method to realize three-dimensional mapping of CDM substructures in extragalactic halos. We have shown that at submillimeter wavelengths, a measurement of astrometric shifts of perturbed multiple images with respect to unperturbed images can break the degeneracy between subhalo mass and position in the line-of-sight to the image if resolved at the scale of an Einstein radius of the perturber. Furthermore, assuming that the tidal radius is approximately equal to the subhalo size, the distance from the center of the macrolens halo can be determined from the size of the region within an image outside which the astrometric shift is suppressed.

Although we have considered a very simple model, the essential features of astrometric shifts will not be dramatically altered even if we consider a more complicated model such as a macrolens perturbed by a number of non-circular subhalos and/or subhalos having a so-called NFW profile (Navarro, Frenk & White 1996). This is because (1) the astrometric shifts caused by a significant number of smaller mass subhalos are canceled out on larger scales if they are not clustered on that scale.

However, several massive perturbers (often not within the image) may distort the images so that the accuracy in measuring the distance to a single perturber along the line-of-sight may become significantly worse. (2) Deviation from a circular symmetry or from an SIS mass profile can affect the astrometric shifts significantly. For instance, if the substructures had an NFW or some other less-cuspy inner profile, the simulated dipole pattern inside the Einstein radius would be less prominent (Inoue & Chiba 2004). However, the generic feature of substructure lensing, i.e., its dependence on the parity of a macrolensed image outside the Einstein radius of a perturber, will probably be unaltered; if the outer density profile of a substructure falls off as fast as an SIS with increasing radius, then we expect similar astrometric shifts to those for an SIS. Even if the outer density profile is shallower than an SIS, we can make a distinction between models with different density profiles and ellipticities from astrometric shifts of a number of internal positions within the source, if the source has a substructure.

We would like to thank the anonymous referee for valuable comments. This work has been supported in Part by a Grant-in-Aid for Scientific Research (15540241) of the Ministry of Education, Culture, Sports, Science and Technology in Japan.

#### REFERENCES

- Barvainis, R. & Ivison, R. 2002, *ApJ*, 571, 712  
 Blain, A. W. 1999, *Astrophys. Space Sci.*, 266, 261  
 Bradac, M., Schneider, P., Steinmetz, M., Lombardi, M., & King, L. J. 2002, *A&A*, 388, 373  
 Chiba, M. 2002, *ApJ*, 565, 17  
 Chiba, M., Minezaki, T., Kashikawa, N., Kataza, H., & Inoue, K. T. 2005, *ApJ*, 627, 53  
 Dalal, N. & Kochanek, C. S. 2002, *ApJ*, 572, 25  
 Dobler, G. & Keeton, R. C. 2005, *MNRAS*, submitted (astro-ph/0502436)  
 Evans, N. W. & Witt, H. J. 2003, *MNRAS*, 345, 1351  
 Inoue, K. T. & Chiba, M. 2003, *ApJL*, 591, L83  
 Inoue, K. T. & Chiba, M. 2005, *ApJ*, 634 in press (astro-ph/0411168)  
 Keeton, C. R. 2003, *ApJ*, 584, 664  
 Keeton, C. R., Gaudi, B.S., & Petters, A. O. 2003, *ApJ*, 598, 138  
 Kormann, R., Schneider, P., & Bartelmann, M. 1994, *A&A*, 284, 285  
 Klypin, A., Kravtsov, A. V., Valenzuela, O., & Prada, F. 1999, *ApJ*, 522, 82  
 Mao, S. & Schneider, P. 1998, *MNRAS*, 295, 587  
 Metcalf, R. B., 2005, *ApJ*, 629, 673  
 Metcalf, R. B. & Madau, P. 2001, *ApJ*, 563, 9  
 Metcalf, R. B. & Zhao, H. 2002, *ApJ*, 567, L5  
 Moore, B., Ghigna, S., Governato, F., Lake, G., Quinn, T., & Stadel, J. 1999, *ApJ*, 524, L19  
 Navarro, J. S., Frenk, C. S. & White, S. D. M. 1996, *ApJ*, 462, 563  
 Wiklind, T. 2003, *ApJ*, 588, 736  
 Wiklind, T. & Alloin D. 2002, in *Gravitational Lensing: An Astrophysical Tool*, ed. F. Courbin & D. Minniti (Berlin:Springer), 124  
 Yonehara, A., Umemura, M. & Susa, H. 2003, *PASJ*, 55, 1059

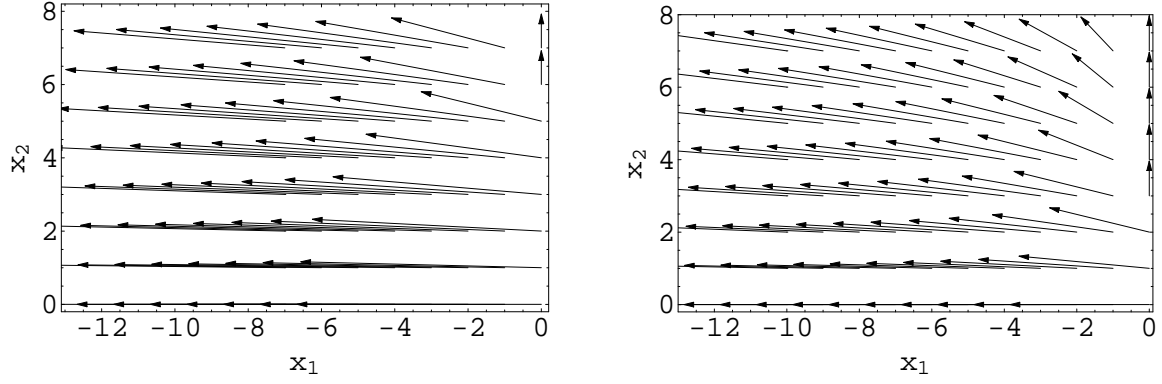


FIG. 2.— Astrometric shifts  $\Delta\mathbf{x}$  for an SIS perturber in a macrolens halo for  $\beta = 0$  (*left*) and those for an SIS perturber in the foreground of a macrolens for  $\beta = 0.5$  (*right*) with respect to images for an unperturbed macrolens in the image plane  $(x_1, x_2)$  aligned to the shear. Both horizontal and vertical axes are normalized by the Einstein radius  $\theta_{Ep}$  of an SIS perturber. We adopt a convergence  $\kappa = 0.38$  and a shear  $\gamma = 0.47$  for the macrolens.

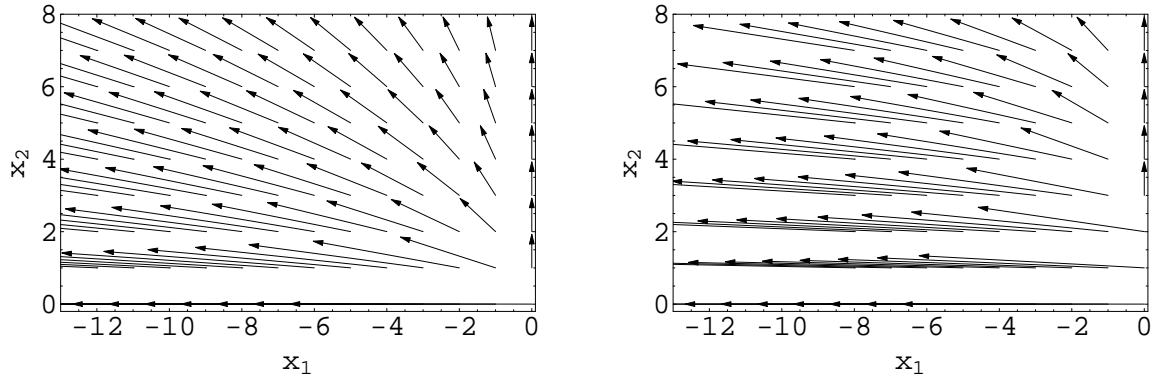


FIG. 3.— Astrometric shifts  $\Delta\mathbf{x}$  for an SIS perturber in the background of a macrolens halo for  $\beta = 0.9$  (*left*) and  $\beta = 0.5$  (*right*) with respect to images for an unperturbed macrolens model. The other parameters are the same as those in Figure 2.

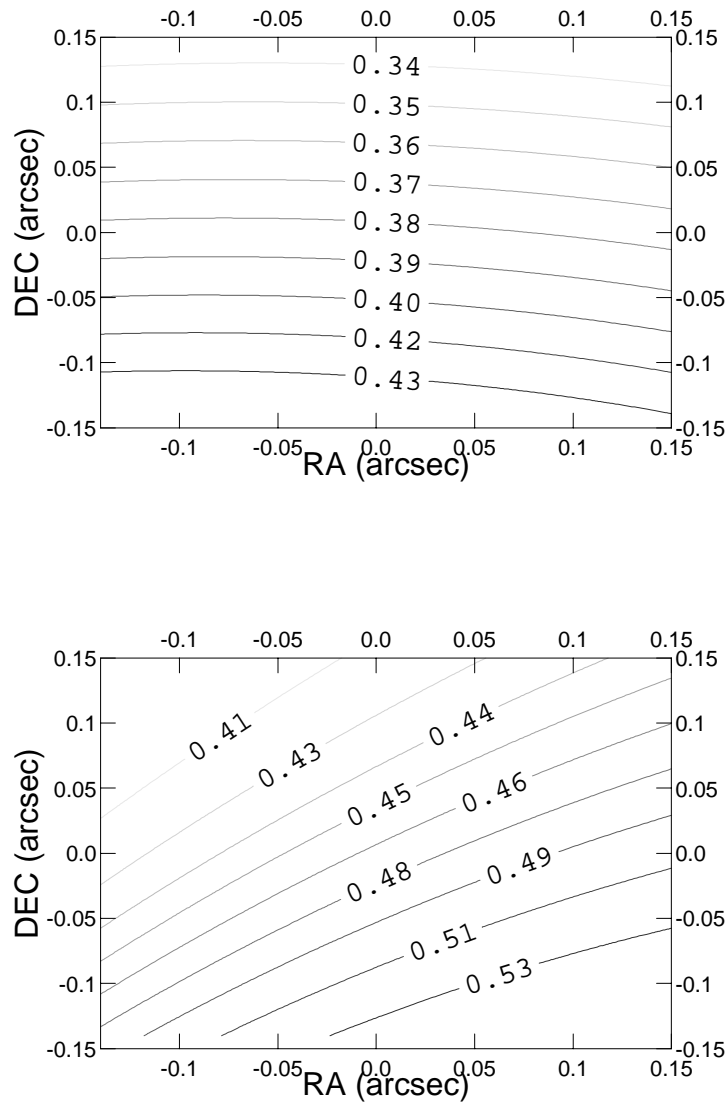


FIG. 4.— Contour plots of  $\kappa$  (*top*) and  $\gamma$  (*bottom*) for our SIE model of B1422+231 in the neighborhood of an SIS perturber (the position is plotted in the top right panel in Figure 1) that is centered at the coordinate center.